Zhou, T., Lv, W., Geng, Y., Xiao, S., Xu, X., Pan, J., Si, B., **Lausch, A.** (2023):
National-scale spatial prediction of soil organic carbon and total nitrogen using long-term optical and microwave satellite observations in Google Earth Engine
Comput. Electron. Agric. **210** , art. 107928

National-scale spatial prediction of soil organic carbon and total nitrogen using long-term optical and microwave satellite observations in Google Earth Engine

Tao Zhou[a, b, c, 1], Wenhao Lv[a, 1], Yajun Geng[a], Shancai Xiao[d], Jie Chen[e], Xiangrui Xu[f], Jianjun Pan[g], Bingcheng Si[a, *] and Angela Lausch[b, c]

a Ludong University, School of Resources and Environmental Engineering, Middle Hongqi Road 186, 264025 Yantai, China

b Humboldt-Universität zu Berlin, Department of Geography, Unter den Linden 6, 10099 Berlin, Germany

c Helmholtz Centre for Environmental Research, Department of Computational Landscape Ecology, Permoserstraße 15, 04318 Leipzig, Germany

d Peking University, College of Urban and Environmental Sciences, Yiheyuan Road 5, 100871 Beijing, China

e Hunan Academy of Agricultural Sciences, Yuanda 2nd Road 560, 410125 Changsha, China

f Zhejiang University City College, School of Spatial Planning and Design, Huzhou Street 51, 31000 Hangzhou, China

g Nanjing Agricultural University, College of Resources and Environmental Sciences, Weigang 1, 210095 Nanjing, China

* Corresponding author.

E-mail address: bing.si@usask.ca (B. Si).

[1] These authors contributed equally to this paper.

Abstract:

Modeling accurate and detailed soil spatial information is essential for environmental modeling, precision soil management and decision-making. In this study, we integrated long-term optical (Sentinel-2) and radar (Sentinel-1) satellite observations via the Google Earth Engine (GEE) platform for high-resolution national-scale digital mapping of soil organic carbon (SOC) and total soil nitrogen (TSN) in Austria. Our soil predictive models based on boosted regression tree (BRT) and regression kriging (RK) methods were constructed from 449 soil samples (0-20 cm) covering the study area in the LUCAS soil database and Sentinel observations synthesized with different time intervals. The different input predictors of these soil predictive models resulted in seven modeling scenarios, and their prediction performance was evaluated by a cross-validation technique. Comparative analysis indicated that satellite sensors, modeling techniques, and SAR data acquisition configurations greatly affected the model outputs. Cross-polarization and co-polarization had similar performance in TSN and SOC predictions, and their combination improved the prediction accuracy. Predictive models based on Sentinel-1 with the "ASCENDING" orbits outperformed the models involving the "DESCENDING" orbits; the prediction accuracy of the former was comparable to models involving two orbital data. The models built by Sentinel-1 and Sentinel-2 performed similarly in predicting SOC (R^2 = 0.51 vs. R^2 = 0.52, respectively) and TSN (their R^2 were both 0.42); their synergistic utilization improved the prediction results. Models involving more years of Sentinel observations on the GEE platform provided more accurate modeling results. The best soil predictive models explained 55% and 45%

of soil variability for SOC and TSN, respectively, both constructed from long-term Sentinel-1/2 observations using the RK method. The overall trends of the mapping results of the models constructed by Sentinel-1 and Sentinel-2 and their combinations were consistent. The predicted digital soil maps displayed high spatial heterogeneity: SOC and TSN—shared similar spatial patterns—were greater in high-altitude central and western regions than other regions. This study provides valuable information for revealing the effects of satellite sensors, modeling techniques and SAR configurations on mapping SOC and TSN.

Keywords: digital soil mapping; Cloud computing; soil properties; Sentinel-1; Sentinel-2

1. Introduction

Humanity is facing grand global challenges such as land degradation, climate change, biodiversity decline, sustainable land management and food security (Fu et al., 2021; Musche et al., 2019). Soil, as the center of the terrestrial ecosystem, provides agricultural needs, supports food production, regulates greenhouse gases, and promotes plant and animal health (Ma et al., 2017; Nussbaum et al., 2018; Zhang et al., 2017). As such, there is an urgent demand for accurate and detailed soil spatial information from local to global scales to respond to the above-mentioned challenges. Information from conventional soil surveys is helpful in this regard, but have been criticized for their subjective and qualitative nature because sustainable management requires quantitative soil information (Fathololoumi et al., 2020; Zeraatpisheh et al., 2019; Zeraatpisheh et al., 2022).

The advances in remote sensing, statistics and geographic information technology have created great potential for improving soil mapping (McBratney et al., 2003; Odhiambo et al., 2020). In this context, digital soil mapping techniques have emerged as a powerful method for producing soil maps at different scales (Azizi et al., 2022; Minasny and McBratney, 2016; Naimi et al., 2022b). Digital soil mapping techniques create spatial soil information systems based on the relationship between soil observations and predictors to predict soil properties at unsampled locations (Wadoux et al., 2019). Environmental data obtained from various sources could be linked to soil properties by digital soil mapping techniques, including digital elevation model (DEM) and its derivatives, satellite imagery, climate and topographic data (Asgari et al., 2020a; Asgari et al., 2020b; Naimi et al., 2022a; Zhou et al., 2020). Currently, the amount and availability of environmental data is growing rapidly, especially for Earth observation (EO) data, which is driving a major shift in soil mapping (Tziolas et al., 2020).

Optical images that are easily accessible and familiar to users are the most commonly used EO data for the digital mapping of soil properties (Poggio and Gimona, 2017). However, the availability of optical images is usually affected by cloud cover and hinders their application in soil mapping. Synthetic aperture radar (SAR) images are not affected by cloud cover, but their application in digital soil mapping has not been well developed (Zhou et al., 2020). Recently, several scholars have explored the feasibility of SAR sensors for soil organic carbon (SOC) and total soil nitrogen (TSN) mapping and demonstrated their usefulness (Yang et al., 2019; Zhou et al., 2022). Moreover, the synergistic advantages of SAR and optical sensors in digital mapping of soil properties have been found by several researchers (Nguyen et al., 2022; Wang et al., 2020b; Zhou et al., 2020), who reported that the application of multi-source sensors improved the mapping accuracy of soil properties. However, this is not the case in a study that synergistically exploited SAR and optical data for SOC mapping (Shafizadeh-Moghadam et al., 2022); and the accuracy of the above SOC predictive models constructed from SAR data is relatively low e.g. in Zhou et al. (2020) (R^2 = 0.22) and Wang et al. (2020b) (R^2 = 0.20). The differring mapping accuracy of these soil predictive models may be caused by the utilization strategies of the SAR data.

The interaction of the SAR signal with the surface depends on various radar system parameters such as band frequency, polarization mode and angle of incidence (Mahdianpari et al., 2017). The band frequency is related to the penetration depth of ground targets, with longer wavelengths penetrating deeper. The sensitivities of SAR systems in different bands to soil and plant parameters vary (Mengen et al., 2021). There are differences in the backscattering characteristics of ground targets under different polarization modes of the SAR system. Multi-polarization SAR systems are able to provide more information about the surface scattering mechanism with the help of different polarization modes in the target area (Kumar et al., 2022). Scientists when using SAR data for soil mapping could be confused by the various possible configurations of these data, such as polarization, band frequency and orbital direction, especially since the configuration affects the ability to predict soil properties. In this context, many scholars have emphasized the importance of studying the impact of SAR data acquisition configuration on

SAR data modeling (DeVries et al., 2020; Hethcoat et al., 2021; Hosseini et al., 2015; Rapinel et al., 2020). However, the relative impact of each acquisition configuration on digital mapping of SOC and TSN remains unknown.

The advent of the big data era for EO and improvements in computing power are facilitating the development of large-scale soil mapping methods (Luo et al., 2022c; Tziolas et al., 2020). The newly released Copernicus satellite series (Sentinel-1/2) provides an excellent opportunity for digital soil mapping to include a comprehensive dataset of high-resolution spatiotemporal information on the land surface (d'Andrimont et al., 2021; Loiseau et al., 2019). Some studies have explicitly suggested that long-term satellite observations may be more powerful than single-date data for soil prediction due to their ability to capture changes in land surface characteristics over time (Fathololoumi et al., 2021; Guo et al., 2021). The inclusion of abundant satellite observations increases model computation time and thus reduces computational efficiency. The complexity of SAR preprocessing, especially long-term SAR satellite observation data, presents an obstacle to its adoption (DeVries et al., 2020). Sentinel satellite sensors have made some contributions to the efficient modeling of soil properties (Agyeman et al., 2023; Zhou et al., 2021), but few studies have used long-term optical and radar Sentinel satellite observations to achieve this goal due to the difficulties in accessing and processing such a large number of satellite imagery.

Cloud-based platforms, such as Google Earth Engine (GEE), can greatly improve the efficiency of image analysis, allowing for the relatively easy integration of disparate satellite data sources. The advent of GEE allows users to access the entire archive of EO data and avoid the need to download and store large amounts of data locally (DeVries et al., 2020; Zhang et al., 2019). The GEE platform can use Google's computational infrastructure to process geospatial data simultaneously, thereby reducing computational time (Tamiminia et al., 2020). The GEE platform has made substantial progress in environmental analysis from regional to global scales, but its application in soil property mapping is still in its infancy (Luo et al., 2022c). The cloud computing platforms like GEE and the open data policies of the Copernicus Project, are now poised to facilitate exploration of the vast datasets of multiple satellite missions to improve soil predictive models based on satellite observations.

In this study, we integrated long-term optical (Sentinel-2) and microwave (Sentinel-1) satellite observations in Austria with the help of GEE to: (1) evaluate the effects of SAR data utilization strategies on soil predictive models (i.e., SOC and TSN); (2) investigate the prediction performance of different satellite sensors and whether optical-SAR data fusion improves mapping accuracy; and (3) evaluate the optimal time window for SOC and TSN mapping in Austria based on long-term satellite observations.

2. Materials and Methods

2.1. Study area

Austria is located in southern Central Europe and the temperate climate zone with a total area of 83,879 km² (Fig. 1). The elevation of Austria is between 115 and 3797 m a.s.l. The west and south are dominated by mountainous landscapes, while the north and northeast are lowland and hilly areas. The mean annual precipitation ranges from 400 mm in the eastern lowlands to nearly 3000 mm in the western Alps (Surer et al., 2014). The mean annual temperature is between 8 and 10°C (Sleziak et al., 2016). About 50% of Austria's area is occupied by forest land, which is primarily dominated by coniferous species (Müller et al., 2013). Agricultural area accounts for about one-third of the country's land area and is mainly composed of cultivated land, permanent grassland and meadow. Cultivated land is mainly located in the east with wheat as the main crop, followed by maize, while the grasslands are mostly in the west. Cambisol, Leptosol and Luvisol are the main soil types (Gentile et al., 2009).

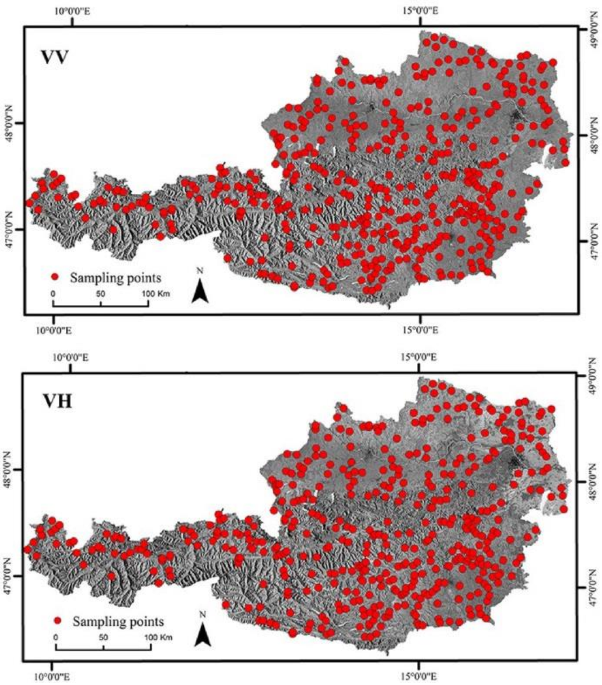

Fig. 1. Long-term composite images of dual-polarized Sentinel-1 with "ASCENDING" orbits (period 1: January–February 2018) and distribution of soil samples.

2.2. Soil dataset

We collected SOC and TSN data from the LUCAS Topsoil Database covering Austria, which was provided from the European Soil Data Center (Orgiazzi et al., 2018; Tóth et al., 2013). As a module of the LUCAS Survey project, LUCAS soil is the largest and most comprehensive soil database representing European soil (Yigini and Panagos, 2016). LUCAS included the soil module for the first time in 2009, providing approximately 20,000 topsoil samples (0-20 cm) collected on different land use types covering 25 Member States (MS) of the European Union (EU) (Fernández-Ugalde et al., 2020b). The sampling locations were selected to represent the landscape features of Europe, with a density of about 1 per 199 km^2 (Schiefer et al., 2016). In the LUCAS 2018 Topsoil Survey, approximately 27,000 soil sampling locations were initially identified, while the final soil module dataset contained data for 18,984 locations; 16,556 sites from the LUCAS 2015 surveys were revisited; part of the new points in the 2015 survey were located at altitudes of 1,000-2,000 m, beyond the scope of the LUCAS 2009/2012 survey (Fernández-Ugalde et al., 2020a; Fernandez-Ugalde et al., 2022). The selection of sample points, soil sampling and analysis methods of soil properties were described in detail by Orgiazzi et al. (2018). The LUCAS soil database records various basic soil properties such as SOC, TSN and pH. (Castaldi et al., 2018). As the most harmonized soil dataset at European scale, the LUCAS soil database has been used to carry out prediction studies of soil properties at different scales (Ballabio et al., 2016; Wadoux, 2019; Wang et al., 2020b). We extracted all soil samples (n = 449) covering Austria from the LUCAS 2018 soil dataset to predict SOC and TSN (Fig. 1).

2.3. Remote sensing data and pre-processing

Sentinel-1 and Sentinel-2 satellites provide C-band SAR images and optical imaging data, respectively. The Sentinel-1 (6-day revisit) satellite supports four operating modes with different resolutions and coverage areas (Yagüe-Martínez et al., 2016). Interferometric Wide Swath Mode (IW) is the main operating mode over land, with a high spatial resolution (5 m × 20 m) and a wide coverage (250 km) (Huang et al., 2018). The Sentinel-2 sensor provides multispectral image (13 spectral bands) data with high spatial resolution (10-60 m) and wide area coverage (swath width of 290 km) at a 5-day interval (Murphy et al., 2016).

We used IW-mode Sentinel-1 SAR imagery with dual polarization (vertical transmit/vertical receive (VV) and vertical transmit/horizontal receive (VH)). All available Sentinel-1 images (from the beginning of dataset availability until 2018) in Austria were accessed and preprocessed on the GEE platform to generate backscatter coefficient in decibels (dB). In the GEE platform, we filtered Sentinel-1 data according to the orbital direction to get Sentinel-1 data with "DESCENDING" and "ASCENDING" orbitals. More details on the steps taken by the GEE platform to process Sentinel-1 data can be found in Singha et al. (2020). To evaluate the optimal time window for soil prediction, all acquired Sentinel-1 images were synthesized in multi-year (all Sentinel-1 images by 2018) and single-year (Sentinel-1 images in 2018) time windows, respectively. We applied a median function to the acquired Sentinel-1 images based on these two time windows to construct long-term composite images of Sentinel-1 for every two-month period. Twelve long-term composite images of Sentinel-1 for six time periods (e.g., period 1: January–

February) were produced over a twelve month period. Long-term composite images are less susceptible to changes in image acquisition conditions than single date imagery (Anchang et al., 2020). Twenty-four Sentinel-1 features were synthesized under each time window, and these long-term composite images from different polarization modes (i.e., VV and VH) and orbital directions were used as input predictors.

There are two levels of Sentinel-2 available in GEE, with the higher-level Sentinel-2 Level 2A product containing orthorectified atmospherically corrected surface reflectance processed using Sen2Cor tool from the Copernicus Scientific Data Hub (Roca et al., 2022; Tian et al., 2021). This study collected all Sentinel-2 surface reflectance data (Level 2A) with cloud cover less than 10% via GEE from when the data was available on GEE to 2018. Similar to Sentinel-1, acquired Sentinel-2 images were processed and analyzed in multi-year and single-year time windows, respectively. Cloud masking was performed using Sentinel-2 QA band that provides cloud state information (Zhang et al., 2019). The median function was used to downscale all Sentinel-2 images, resulting in Sentinel-2 composite images at different time windows (Ghorbanian et al., 2020). The 10 extracted Sentinel-2 bands (i.e., bands 2-8a, 11, and 12) were used as explanatory variables to construct soil predictive models, which are widely used in soil mapping (Gholizadeh et al., 2018; Vaudour et al., 2019). In total, 68 Sentinel-1/2 derived predictors composed of single-year and multi-year composite images were used for further modeling and analysis of SOC and TSN (Table 1).

Table 1. Summary description of Sentinel-1/2-derived predictors synthesized from long-term satellite observations.

Sensors	Number of features	Description
Sentinel-1	12	Backscatter coefficient in "ASCENDING" orbit
Sentinel-1	12	Backscatter coefficient in "DESCENDING" orbit
Sentinel-1	12	Backscatter coefficient in VH polarization
Sentinel-1	12	Backscatter coefficient in VV polarization
Sentinel-1	24	All available Sentinel-1 derived predictors
Sentinel-2	10	Sentinel-2 bands (i.e., bands 2-8a, 11, and 12)

2.4. Predictive models

2.4.1. Boosted regression trees

The boosted regression tree (BRT) model is a combination of statistical methods and machine learning techniques with the advantages of two algorithms (i.e., boosting and regression trees) (Elith et al., 2008). It is a powerful regression modeling technique that can effectively select relevant variables and determine the most important input variables (Arabameri et al., 2019). This model is known to have several advantages, including low sensitivity to overfitting and stable predictive power (Wang et al., 2018). The BRT model has been widely used to solve various ecological modeling problems, especially the spatial prediction of soil properties (Lamichhane et al., 2019; Zhang et al., 2017). Three main parameters need to be set for BRT modeling: the learning rate, the number of trees and the tree complexity (Ottoy et al., 2017). We used the "caret" package in R software to perform a grid search to optimize these parameters (Forkuor et al., 2017; Kuhn, 2008). The combination of these parameters that produced the lowest prediction error was set for final analysis. The BRT prediction method was implemented in the R software using the "gbm" packages.

2.4.2. Regression kriging

Regression kriging (RK) is the most commonly used hybrid spatial interpolation and modeling method that integrates regression and interpolation techniques in a single step (Ma et al., 2017). In the RK method, the target soil properties are explained by auxiliary variables through a regression model and the regression residuals are described by spatial autocorrelation using kriging techniques (Hengl et al., 2007). This method has been reported to improve model performance compared to ordinary kriging (Hengl et al., 2004). The RK model was implemented using the "fit.gstatModel" function of the "GSIF" package in the R software; it combines regression and residual kriging in a single step (Llamas et al., 2020; Zhang et al., 2020).

2.5. Model performance evaluation

Soil predictive models were constructed from different input variables, resulting in seven modeling scenarios (Scenario 1: long-term composite images from VV polarization; Scenario 2: long-term composite images from VH polarization; Scenario 3: long-term composite images of Sentinel-1 with "ASCENDING" orbits; Scenario 4: long-term composite images of Sentinel-1 with "DESCENDING" orbits; Scenario 5: all available Sentinel-1 derived predictors; Scenario 6: all available Sentinel-2 derived predictors; Scenario 7: combination of SAR and optical data (Sentinel-1+ Sentinel-2)). The performance of the above models was evaluated by 10-fold cross-validation. The following validation indices were calculated to compare and evaluate model performance: the root mean square error (RMSE), the mean absolute error (MAE) and the coefficient of determination (R^2).

3. Results

3.1. Descriptive statistics of SOC and TSN

The statistics of the soil properties are presented in Table 2. The mean values of SOC and TSN in the topsoil were 80.06 g/kg (median: 47.50 g/kg) and 5.20 g/kg (median: 4.00 g/kg), respectively. SOC ranged from 3.10 to 723.90 g/kg and TSN ranged from 0.40 to 46.50 g/kg. The above soil properties showed a strongly skewed distribution; the skewness coefficients for SOC and TSN were 2.70 and 3.36, respectively. We therefore applied the natural logtransformation to those soil properties; the skewness coefficients of SOC and TSN dropped to 0.29 and 0.17, respectively.

Table 2 Statistical summary of SOC and TSN in the study area (n = 449).

	Minimum	Maximum	Mean	Median	Standard deviation (SD)	Skewness
SOC	3.10	723.90	80.06	47.50	89.49	2.70
LnSOC	1.13	6.58	3.93	3.86	0.92	0.29
TSN	0.40	46.50	5.20	4.00	4.34	3.36
LnTSN	-0.91	3.83	1.40	1.38	0.68	0.17

Notes: LnSOC, log-transformed SOC; LnTSN, log-transformed TSN.

3.2. Predictive performance

The performance of BRT and RK models in predicting SOC and TSN based on multi-year and single-year composite data under the seven scenarios is shown in Table 3. The comparative analysis of the mapping accuracy of different modeling scenarios showed that the choice of satellite sensors, modeling methods, polarization modes, orbital directions and time window greatly affected the output of soil predictive models. For example, for the two modeling techniques used, RK performed better than BRT in SOC and TSN mapping from Scenario 1 to Scenario 7. This was confirmed by higher R^2 and lower RMSE and MAE values when SOC (R^2 values in the range of 0.40 to 0.55 for different scenarios) and TSN (R^2 values in the range of 0.37 to 0.45 for different scenarios) were predicted by RK.

The results showed that the SOC and TSN predictive models constructed by Sentinel-1 had obdvious differences in accuracy under various SAR data-acquisition configurations. Scenarios 1 and 2, -both constructed from only a single polarization- showed relatively poor performance; the two polarization modes (i.e., VV and VH) had similar performance in mapping SOC and TSN using the RK model. The combined polarization (Scenario 5) effectively improved the mapping accuracy of SOC and TSN compared to Scenarios 1 and 2; their relative improvements (in terms of R^2) compared to the RK-based modeling scenarios without VV polarization input were 6% and 5%, respectively. SOC and TSN were better predicted by Sentinel-1 images with "ASCENDING" orbit than experimental scenarios with "DESCENDING" orbit. The accuracy of the experimental scenario with the "ASCENDING" orbit closely followed Scenario 5 (all available Sentinel-1 predictors), while the experimental scenario with the "DESCENDING" orbit performed the poorest of all scenarios.

Among Sentinel-1/2-based experimental scenarios, Scenario 6 constructed by Sentinel-2 had an overall similar predictive performance to Sentinel-1-based experimental scenarios; their best prediction accuracies for SOC (R^2 = 0.52 vs. R^2 = 0.51, respectively) and TSN (R^2 = 0.42) were very close. Scenario 7, constructed from the fusion of SAR and optical data, improved mapping accuracy compared to soil predictive models based on a single sensor; when Sentinel-1 and Sentinel-2 were fused, the R^2 of the SOC and TSN predictive models using the RK method increased from 0.51 to 0.55 and from 0.42 to 0.45, respectively; moreover, soil predictive models based on SAR and optical data achieved the highest accuracy.

Overall, more years of synthetic images in all experimental scenarios provided more accurate SOC and TSN prediction results. This result suggests that choosing an appropriate time window for satellite-based soil predictive models is very important to effectively model SOC and TSN. SOC was more successfully predicted than TSN for all modeling scenarios. The best performance was obtained from the SOC and TSN models fitted by all available Sentinel-1/2-derived predictors (Scenario 7) among all modeling scenarios, with R^2 = 0.55 and R^2 = 0.45 for SOC and TSN predictions, respectively. The R^2 values of the SOC predictive models constructed by Sentinel-1/2 indicated that these models could explain approximately 51% and 52% of the SOC variation, respectively, and together explained 55% of the SOC variability. Meanwhile, the RK models in Scenario 5 (Sentinel-1), Scenario 6 (Sentinel-2) and Scenario 7 (all available Sentinel-1/2 predictors) explained 42%, 42% and 45% of the TSN variability, respectively.

Table 3 Accuracy results of predicting SOC and TSN based on multi-year and single-year composite images under seven scenarios.

Modeling technique	Model	SOC			TSN		
		MAE	RMSE	R^2	MAE	RMSE	R^2
BRT	Scenario 1						
	single-year	0.57	0.75	0.34	0.46	0.60	0.23
	multi-year	0.55	0.73	0.38	0.45	0.59	0.27
	Scenario 2						
	single-year	0.60	0.78	0.30	0.47	0.62	0.20
	multi-year	0.56	0.73	0.37	0.45	0.59	0.25
	Scenario 3						
	single-year	0.57	0.74	0.36	0.45	0.59	0.26
	multi-year	0.54	0.71	0.41	0.43	0.57	0.31
	Scenario 4						
	single-year	0.63	0.81	0.24	0.47	0.62	0.18
	multi-year	0.60	0.77	0.31	0.46	0.60	0.23
	Scenario 5						
	single-year	0.56	0.74	0.36	0.45	0.59	0.26
	multi-year	0.54	0.71	0.41	0.43	0.57	0.31
	Scenario 6						
	single-year	0.53	0.71	0.41	0.44	0.59	0.26
	multi-year	0.53	0.71	0.41	0.43	0.59	0.27
	Scenario 7						
	single-year	0.52	0.70	0.43	0.43	0.58	0.29
	multi-year	0.51	0.69	0.45	0.43	0.57	0.31
RK	Scenario 1						
	single-year	0.52	0.68	0. 45	0.39	0.53	0. 39
	multi-year	0.50	0.66	0.48	0.39	0.53	0. 40
	Scenario 2						
	single-year	0.52	0.69	0.45	0. 39	0. 53	0. 38
	multi-year	0.51	0.67	0.48	0. 39	0. 53	0. 40
	Scenario 3						
	single-year	0. 51	0. 67	0. 47	0. 39	0.53	0.40
	multi-year	0. 50	0. 66	0. 49	0. 39	0. 52	0. 41
	Scenario 4						
	single-year	0. 55	0. 71	0.40	0.40	0. 54	0. 37
	multi-year	0. 53	0. 68	0. 45	0. 39	0. 53	0. 40
	Scenario 5						
	single-year	0.51	0.67	0. 47	0.39	0. 53	0. 40
	multi-year	0.49	0. 65	0. 51	0.38	0. 52	0. 42

Scenario 6						
single-year	0.50	0. 64	0. 51	0. 39	0. 52	0.41
multi-year	0.49	0.64	0.52	0. 38	0. 52	0. 42
Scenario 7						
single-year	0. 48	0. 62	0. 54	0. 38	0. 51	0. 43
multi-year	0. 47	0. 62	0. 55	0.38	0.51	0.45

3.3. Importance of auxiliary variables

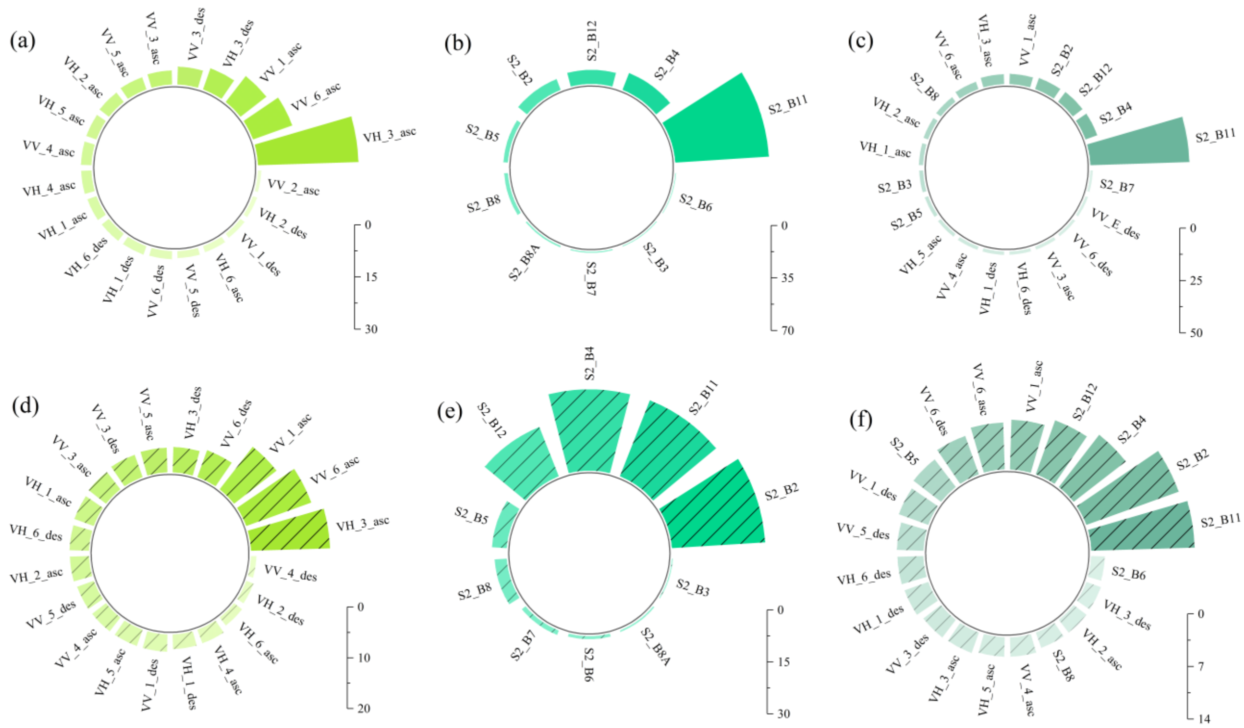

Fig. 2. Importance of auxiliary variables in predicting SOC and TSN using BRT model based on different experimental scenarios. (a)–(c) correspond to the importance results of modeling scenarios 5 to 7 in predicting SOC, respectively; (d)–(f) correspond to the importance results of modeling scenarios 5 to 7 in predicting TSN, respectively; VV_1_asc to VV_6_asc correspond to long-term composite images of VV polarization with "ASCENDING" orbits from six time periods, respectively; VV_1_des to VV_6_des correspond to long-term composite images of VV polarization with "DESCENDING" orbits from six time periods, respectively; S2_B2 to S2_B12 are the spectral bands of Sentinel-2 data.

The relative importance of explanatory variables in predicting SOC and TSN, which was estimated by the BRT algorithm, is shown in Fig. 2. The variable importance rankings of the two soil attributes were different, revealing different dominating environmental variables in the two soil predictive models. VH_3_asc, VV_6_asc, VV_1_asc and VV_3_des, all located in the top five most important predictors of the SOC and TSN predictive models built by Sentinel-1, together accounting for 56% and 45% of the total relative importance, respectively. S2_B11, S2_B4, S2_B12 and S2_B2 had the largest contributions in the SOC and TSN predictive models established by Sentinel-2, with the sum of their importance being 92% and 89%, respectively. These Sentinel-2 derived predictors also ranked in the top four for SOC and TSN models utilizing the combination of Sentinel-1 and Sentinel-2. Among the models built by Sentinel-1/2, only one of the top five most important predictors came from Sentinel-1, suggesting that Sentinel-2 had a greater impact on the models than Sentinel-1; the total relative importance of Sentinel-2-derived variables in the SOC and TSN predictive models was 72% and 52%, respectively.

3.4. Predicted national maps of SOC and TSN

We produced high-resolution digital soil maps for SOC and TSN in Austria using the BRT and RK models under different experimental scenarios (Figs. 3-4). The spatial patterns of the mapping results of the soil predictive models under these two modeling techniques were generally similar, but the spatial details were slightly different. We observed that the overall trends in the mapping results of soil predictive models built by Sentinel-1 and Sentinel-2 and their combinations were consistent, although the two systems had different image characteristics, information content, and imaging techniques. Meanwhile, the mapping results of the SOC and TSN predictive models shared similar spatial patterns. The average values of SOC mapped by Scenario 5 (Sentinel-1), Scenario 6 (Sentinel-2) and Scenario 7 (Sentinel-1/2) using the RK model were 63.98 g/kg (SD: 38.77 g/kg), 65.08 g/kg (SD: 44.28 g/kg) and 63.73 g/kg (SD: 45.06 g/kg), respectively. The mean and SD values of the predicted TSN using the RK model were 4.41 and 1.93 g/kg for Scenario 5, 4.50 and 2.18 g/kg for Scenario 6, and 4.47 and 2.32 g/kg for Scenario 7, respectively.

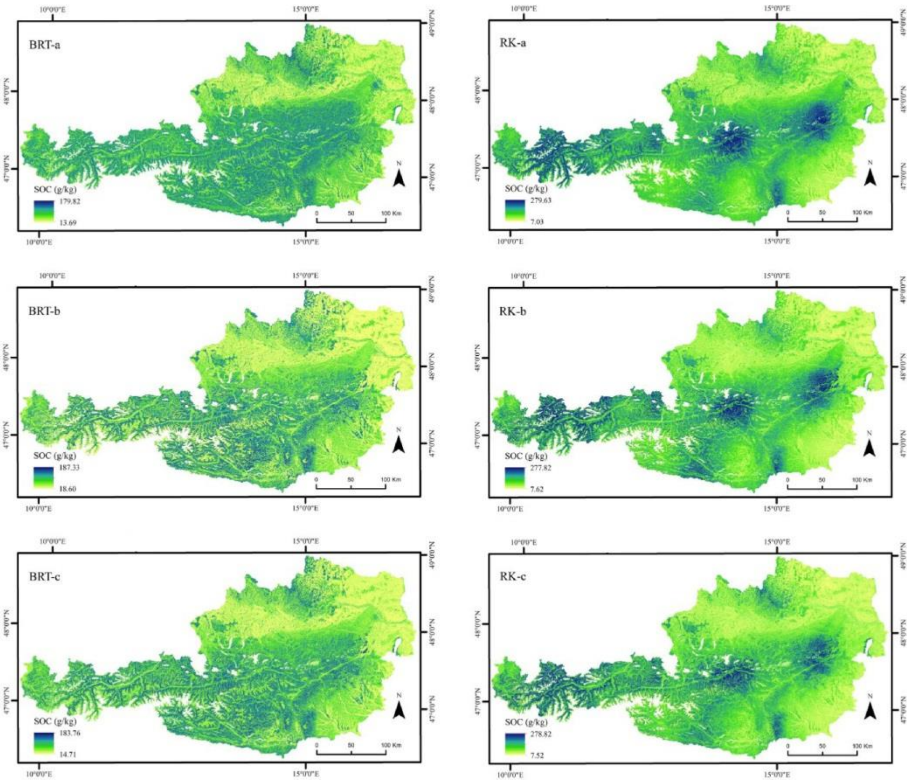

Fig. 3. Maps of SOC produced using BRT and RK models based on different experimental scenarios. RK-a to RK-c correspond to the predicted maps of modeling scenarios 5 to 7 based on the RK model, respectively; BRT-a to BRT-c correspond to the predicted maps of modeling scenarios 5 to 7 based on the BRT model, respectively; Scenario 5 included all available Sentinel-1 derived predictors; Scenario 6 included all available Sentinel-2 derived predictors; Scenario 7 included all available Sentinel-1/2 derived predictors.

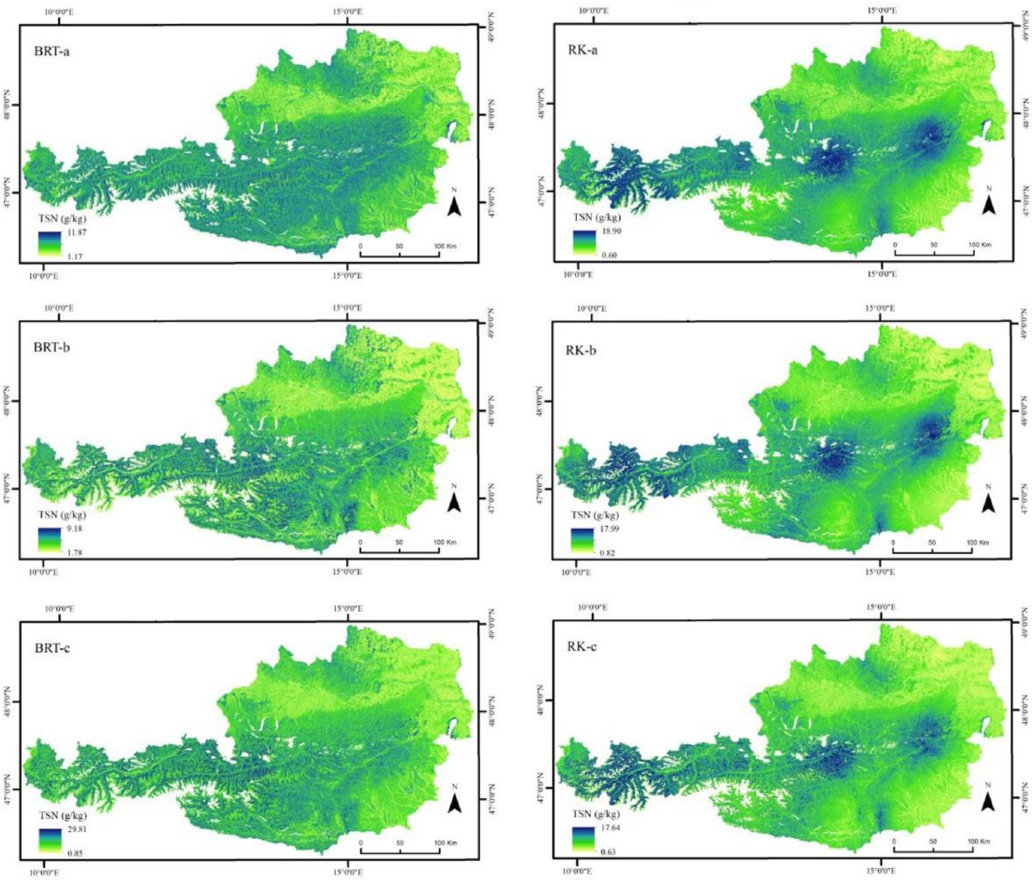

Fig. 4. Maps of TSN produced using BRT and RK models based on different experimental scenarios. RK-a to RK-c correspond to the predicted maps of modeling scenarios 5 to 7 based on the RK model, respectively; BRT-a to BRT-c correspond to the predicted maps of modeling scenarios 5 to 7 based on the BRT model, respectively; Scenario 5 included all available Sentinel-1 derived predictors; Scenario 6 included all available Sentinel-2 derived predictors; Scenario 7 included all available Sentinel-1/2 derived predictors.

4. Discussion

4.1. Performance of different modeling scenarios in predicting SOC and TSN

Our comparative analysis based on different modeling scenarios showed that the choice of sensors and modeling techniques, as well as the SAR utilization strategies (i.e., polarization modes, orbital directions and time window) greatly affected the output of soil predictive models (Table 3). Our results showed that VV and VH polarizations exhibited similar performance in mapping SOC and TSN. Combined polarizations had more accurate prediction results than single polarizations. Many scholars reported that multi-polarization contains more information about the target scattering mechanism than single-polarization (Irwin et al., 2018; Liu et al., 2021). In our study, SOC and TSN were better predicted by Sentinel-1 images of the "ASCENDING" orbit than scenarios involving the "DESCENDING" orbit. Moreover, the experimental scenario with "ASCENDING" orbital data had similar prediction performance to Scenario 5 constructed by all available Sentinel-1 predictors. Some scholars have emphasized the differences in the backscatter and scattering mechanisms in different orbital directions of radar sensors (Elfadaly et al., 2020; Mahdavi et al., 2019). The prediction accuracy based on long-term Sentinel-1 observations was superior to previous studies utilizing multitemporal SAR data (Zhou et al., 2020).

Our study demonstrated the feasibility and reliability of SOC and TSN mapping using long-term synthetic Sentinel-1 and Sentinel-2 data. This was also supported by Wang et al. (2021) who emphasized the usefulness of Sentinel-1 and Sentinel-2 data in soil prediction. We found that the fusion of SAR and optical data improved the mapping accuracy (Table 3). The observed R^2 values were higher than previous studies based on Sentinel-1 and Sentinel-2 sensors (Li et al., 2021; Zhou et al., 2020). Similar to our results, Nguyen et al. (2022) also reported the potential of combining SAR and optical data to improve accuracy. However, Shafizadeh-Moghadam et al. (2022) found that the synergistic use of Sentinel-1 and Sentinel-2 did not improve accuracy. Various environmental data (e.g., climate, relief and land use) directly or indirectly related to soil formation processes in nature have been widely used to map SOC content from regional to global scales (Chen et al., 2022). Remote sensing technology can obtain rich land surface information for SOC mapping in an effective, fast, frequent and economical way (Odebiri et al., 2021; Yang et al., 2021). Similar to our study, many studies have explored the use of EO data with different characteristics in SOC mapping to improve the utility and performance of EO data without considering other environmental data such as climate and topography (Gholizadeh et al., 2018; Luo et al., 2022a; Odebiri et al., 2022b; Shi et al., 2022). It is expected that the SOC predictive model can be improved when other influential environmental data are included in this study.

In this study, the GEE platform provided good support for efficient soil property modeling. We relied on the GEE platform to maximize the use of effective pixels from Sentinel-1 and Sentinel-2 data. Our results showed that soil predictive models involving more years of composite images from the GEE achieved more accurate prediction results than models with only one year of composite images. The advantages of long-term satellite observations could be explained by their ability to capture changes in land surface characteristics over time (Maynard and Levi, 2017).

Recent studies using the GEE platform for soil mapping have revealed its great potential in soil prediction (Luo et al., 2022b; Luo et al., 2022c). However, these studies only used optical satellite imagery to train the models. Our results revealed that both radar Sentinel-1 and multispectral Sentinel-2 have great potentials in predicting soil properties, especially the former in areas prone to cloud cover.

The prediction accuracy of Scenario 7 (all available Sentinel-1/2 predictors) was the highest among all modeling strategies. The best soil predictive models with the highest R^2 explained 55% and 45% of soil variability for SOC and TSN, respectively. The prediction accuracy of soil properties in this study based solely on long-term optical and radar satellite observations from the GEE platform was comparable to previous studies using topsoil LUCAS data and multisource environmental variables including satellite-derived variables. For example, the R^2 values of SOC and TSN predictive models constructed from long-term Sentinel-1/2 satellite observations in this study were not inferior to those of soil predictive models constructed in Switzerland (Zhou et al., 2021) and France (Wadoux, 2019) based on multi-source environmental data.

4.2. Importance of predictors

Optical images, which are more accessible and familiar to users, are the most commonly used remote sensing data for soil mapping. In our study, Sentinel-1 backscatter bands and Sentinel-2 derived predictors were found to be useful auxiliary variables for mapping SOC and TSN (Fig. 2). For the models constructed by Sentinel-1/2, Sentinel-2 had a larger impact than Sentinel-1 in SOC and TSN predictive models. Sentinel-2 derived predictors were given a sum of relative importance of 72% and 52% in the SOC and TSN predictive models, respectively. Many authors have highlighted the importance of various optical satellite images with different characteristics in predicting soil properties at different scales (Fathololoumi et al., 2020; Odebiri et al., 2022a; Vågen et al., 2016). Four of the top five most important predictors for the models based on all satellite-derived predictors were Sentinel-2 spectral bands. Vegetation cover was found to be highly related to the distribution pattern of soil properties near the topsoil (Wan et al., 2019; Zhang et al., 2018). As reported by Maynard and Levi (2017) and Yang et al. (2019), vegetation and soil coexist as part of the feedback system and the soil-vegetation relationship helps to assist satellite imagery to predict soil properties. Some researchers have used reflectance or vegetation indices derived from Sentinel-2 data as a proxy for vegetation cover to develop soil predictive models (Guo et al., 2021; He et al., 2021).

Unlike previous studies that only focused on optical data, our results revealed that both long-term optical (Sentinel-2) and radar (Sentinel-1) observations have powerful predictive capabilities for soil properties. Sentinel-1 also played an important role in our prediction models (Fig. 2), and comparable prediction performance to Sentinel-2 was observed in the SOC and TSN predictive models (Table 3). VV and VH backscatter images derived from Sentinel-1 were identified as influential predictors. This was supported by other soil mapping studies that revealed the importance of Sentinel-1 backscatter in predicting soil properties (Domenech et al., 2020). Nguyen et al. (2022) reported that Sentinel-1 derived variables played an important role in SOC prediction due to their ability to capture the characteristics of short-term variability in vegetation.

Our results also showed that multi-year satellite observations were more influential than single-year composite images. The GEE platform has been reported to have an important contribution to the efficient modeling of soil properties (Luo et al., 2022a). Tamiminia et al. (2020) reviewed the application status of the GEE platform and found that only 14 of the 349 papers using GEE were related to soil research. The GEE platform hosts vast amounts of remote sensing data, such as the global Sentinel and Landsat archives, and provides analytics-ready satellite products that allow for the relatively easy integration of disparate geospatial data (Wang et al., 2020a). The benefits that the development of GEE has brought to the field of soil mapping cannot be underestimated.

4.3. National-scale maps of SOC and TSN in Austria

The predicted soil maps showed a highly heterogeneous spatial pattern, that is broadly similar with previous digital soil products implemented at the European or global scale (Ballabio et al., 2019; Hengl et al., 2017). However, these existing digital soil maps have a relatively low resolution, preventing end users from understanding the local-scale variation of soil properties. In this study, the overall trends in the predicted maps for radar Sentinel-1 and optical Sentinel-2 and their combinations were consistent, although the two systems had different image characteristics, information content, and imaging techniques. Meanwhile, SOC and TSN, having similar spatial patterns, showed significant spatial variation across different biogeographic regions (Figs. 3-4). Similar findings were also observed in other studies (Jeong et al., 2017; Peng et al., 2014), as there is inherently a strong positive correlation between SOC and TSN (Ma et al., 2018; Oduor et al., 2018).

Generally, high SOC and TSN content mainly occurred in the central and western part of the study area with high altitude, where the land was mostly covered by natural vegetation (woodland and grassland) and was less affected by human disturbance. These areas were characterized by a cold and humid climate and high vegetation coverage, which is conducive to carbon and nitrogen accumulation in the soil. Lower SOC and TSN concentrations were mainly distributed in the low-altitude eastern and northern regions dominated by cultivated land and artificial areas, where the soil was often disturbed by human activities. The predicted values of SOC and TSN in the northern mountainous areas were greater at higher altitudes. These results confirmed that topographic variables, vegetation cover and climate conditions are the main drivers of soil carbon and nitrogen distribution. This was also found in other soil mapping studies (Jeong et al., 2017; Liang et al., 2019) and is consistent with the predictor importance results described above.

5. Conclusions

In this study, we integrated long-term optical and radar Sentinel observations via GEE for high-resolution national-scale digital mapping of soil properties (SOC and TSN) in Austria. The main conclusions are as follows:

- Our results indicated that satellite sensors, modeling techniques, and SAR data acquisition configurations have a significant impact on the output of the SOC and TSN predictive models.
- Overall, VV and VH polarizations performed similarly in predicting SOC and TSN; combined polarizations produced more accurate output results than single polarizations. Sentinel-1 prediction models based on "ASCENDING" orbits outperformed models

involving "DESCENDING" orbits; the prediction accuracy of the former was comparable to models involving two orbital data.

- Soil predictive models involving more years of Sentinel observations from the GEE platform yielded more accurate predictions. Our study highlighted the enormous potential of the GEE platform for large-scale soil mapping.
- Models based on optical Sentinel-2 and radar Sentinel-1 performed similarly in predicting SOC and TSN; their synergistic utilization improved the mapping accuracy. Long-term Sentinel observation-derived variables have a powerful ability to model national-scale SOC and TSN.
- Our most accurate soil predictive models explained 55% and 45% of soil variability for SOC and TSN, respectively; they were both constructed from long-term Sentinel-1/2 observations using the RK method.
- The predicted soil maps showed high spatial heterogeneity, in which SOC and TSN shared similar spatial patterns and had high values in the central and western regions at high altitudes.

Acknowledgments

The authors particularly thank the European Soil Data Center for its support of soil data. First author thanks the China Scholarship Council for its financial support.

References

Agyeman, P.C., Borůvka, L., Kebonye, N.M., Khosravi, V., John, K., Drabek, O., Tejnecky, V., 2023. Prediction of the concentration of cadmium in agricultural soil in the Czech Republic using legacy data, preferential sampling, Sentinel-2, Landsat-8, and ensemble models. J Environ Manage 330, 117194.

Anchang, J.Y., Prihodko, L., Ji, W., Kumar, S.S., Ross, C.W., Yu, Q., Lind, B., Sarr, M.A., Diouf, A.A., Hanan, N.P., 2020. Toward Operational Mapping of Woody Canopy Cover in Tropical Savannas Using Google Earth Engine. Frontiers in Environmental Science 8.

Arabameri, A., Yamani, M., Pradhan, B., Melesse, A., Shirani, K., Tien Bui, D., 2019. Novel ensembles of COPRAS multi-criteria decision-making with logistic regression, boosted regression tree, and random forest for spatial prediction of gully erosion susceptibility. Science of The Total Environment 688, 903-916.

Asgari, N., Ayoubi, S., Demattê, J.A.M., Jafari, A., Safanelli, J.L., Silveira, A.F.D.D., 2020a. Digital mapping of soil drainage using remote sensing, DEM and soil color in a semiarid region of Central Iran. Geoderma Regional 22, e00302.

Asgari, N., Ayoubi, S., Jafari, A., Demattê, J.A.M., 2020b. Incorporating environmental variables, remote and proximal sensing data for digital soil mapping of USDA soil great groups. International Journal of Remote Sensing 41(19), 7624-7648.

Azizi, K., Ayoubi, S., Nabiollahi, K., Garosi, Y., Gislum, R., 2022. Predicting heavy metal contents by applying machine learning approaches and environmental covariates in west of Iran. Journal of Geochemical Exploration 233, 106921.

Ballabio, C., Lugato, E., Fernández-Ugalde, O., Orgiazzi, A., Jones, A., Borrelli, P., Montanarella, L., Panagos, P., 2019. Mapping LUCAS topsoil chemical properties at European scale using Gaussian process regression. Geoderma 355, 113912.

Ballabio, C., Panagos, P., Monatanarella, L., 2016. Mapping topsoil physical properties at European scale using the LUCAS database. Geoderma 261, 110-123.

Castaldi, F., Chabrillat, S., Jones, A., Vreys, K., Bomans, B., Van Wesemael, B., 2018. Soil Organic Carbon Estimation in Croplands by Hyperspectral Remote APEX Data Using the LUCAS Topsoil Database. Remote Sensing 10(2).

Chen, S., Arrouays, D., Leatitia Mulder, V., Poggio, L., Minasny, B., Roudier, P., Libohova, Z., Lagacherie, P., Shi, Z., Hannam, J., Meersmans, J., Richer-de-Forges, A.C., Walter, C., 2022. Digital mapping of GlobalSoilMap soil properties at a broad scale: A review. Geoderma 409, 115567.

d'Andrimont, R., Verhegghen, A., Lemoine, G., Kempeneers, P., Meroni, M., van der Velde, M., 2021. From parcel to continental scale – A first European crop type map based on Sentinel-1 and LUCAS Copernicus in-situ observations. Remote Sensing of Environment 266, 112708.

DeVries, B., Huang, C., Armston, J., Huang, W., Jones, J.W., Lang, M.W., 2020. Rapid and robust monitoring of flood events using Sentinel-1 and Landsat data on the Google Earth Engine. Remote Sensing of Environment 240, 111664.

Domenech, M.B., Amiotti, N.M., Costa, J.L., Castro-Franco, M., 2020. Prediction of topsoil properties at field-scale by using C-band SAR data. International Journal of Applied Earth Observation and Geoinformation 93, 102197.

Elfadaly, A., Abate, N., Masini, N., Lasaponara, R., 2020. SAR Sentinel 1 Imaging and Detection of Palaeo-Landscape Features in the Mediterranean Area, Remote Sensing.

Elith, J., Leathwick, J.R., Hastie, T., 2008. A working guide to boosted regression trees. J Anim Ecol 77(4), 802-813.

Fathololoumi, S., Vaezi, A.R., Alavipanah, S.K., Ghorbani, A., Saurette, D., Biswas, A., 2020. Improved digital soil mapping with multitemporal remotely sensed satellite data fusion: A case study in Iran. Science of The Total Environment 721, 137703.

Fathololoumi, S., Vaezi, A.R., Alavipanah, S.K., Ghorbani, A., Saurette, D., Biswas, A., 2021. Effect of multi-temporal satellite images on soil moisture prediction using a digital soil mapping approach. Geoderma 385, 114901.

Fernández-Ugalde, O., Ballabio, C., Lugato, E., Scarpa, S., Jones, A.J.P.O.o.t.E.U., 2020a. Assessment of changes in topsoil properties in LUCAS samples between 2009/2012 and 2015 surveys. 11-12.

Fernández-Ugalde, O., Jones, A., Meuli, R.G., 2020b. Comparison of sampling with a spade and gouge auger for topsoil monitoring at the continental scale. Eur J Soil Sci 71(2), 137-150.

Fernandez-Ugalde, O., Scarpa, S., Orgiazzi, A., Panagos, P., Van Liedekerke, M., Marechal, A., Jones, A., 2022. LUCAS 2018 Soil Module.

Forkuor, G., Hounkpatin, O.K.L., Welp, G., Thiel, M., 2017. High Resolution Mapping of Soil Properties Using Remote Sensing Variables in South-Western Burkina Faso: A Comparison of Machine Learning and Multiple Linear Regression Models. PLoS One 12(1), e0170478.

Fu, B., Liu, Y., Li, Y., Wang, C., Li, C., Jiang, W., Hua, T., Zhao, W., 2021. The research priorities of Resources and Environmental Sciences. Geography and Sustainability 2(2), 87-94.

Gentile, A.R., Barceló-Cordón, S., Liedekerke, M., 2009. Soil Country Analyses Austria. European Commission, Joint Research Centre-Institute for Environment and Sustainability, EUR 23959EN.

Gholizadeh, A., Žižala, D., Saberioon, M., Borůvka, L., 2018. Soil organic carbon and texture retrieving and mapping using proximal, airborne and Sentinel-2 spectral imaging. Remote Sensing of Environment 218, 89-103.

Ghorbanian, A., Kakooei, M., Amani, M., Mahdavi, S., Mohammadzadeh, A., Hasanlou, M., 2020. Improved land cover map of Iran using Sentinel imagery within Google Earth Engine and a novel automatic workflow for land cover classification using migrated training samples. ISPRS Journal of Photogrammetry and Remote Sensing 167, 276-288.

Guo, L., Fu, P., Shi, T., Chen, Y., Zeng, C., Zhang, H., Wang, S., 2021. Exploring influence factors in mapping soil organic carbon on low-relief agricultural lands using time series of remote sensing data. Soil and Tillage Research 210, 104982.

He, X., Yang, L., Li, A., Zhang, L., Shen, F., Cai, Y., Zhou, C., 2021. Soil organic carbon prediction using phenological parameters and remote sensing variables generated from Sentinel-2 images. Catena 205, 105442.

Hengl, T., Heuvelink, G.B.M., Rossiter, D.G., 2007. About regression-kriging: From equations to case studies. Comput. Geosci. 33(10), 1301-1315.

Hengl, T., Heuvelink, G.B.M., Stein, A., 2004. A generic framework for spatial prediction of soil variables based on regression-kriging. Geoderma 120(1), 75-93.

Hengl, T., Mendes de Jesus, J., Heuvelink, G.B.M., Ruiperez Gonzalez, M., Kilibarda, M., Blagotić, A., Shangguan, W., Wright, M.N., Geng, X., Bauer-Marschallinger, B., Guevara, M.A., Vargas, R., MacMillan, R.A., Batjes, N.H., Leenaars, J.G.B., Ribeiro, E., Wheeler, I., Mantel, S., Kempen, B., 2017. SoilGrids250m: Global gridded soil information based on machine learning. PLoS One 12(2), e0169748.

Hethcoat, M.G., Carreiras, J.M.B., Edwards, D.P., Bryant, R.G., Quegan, S., 2021. Detecting tropical selective logging with C-band SAR data may require a time series approach. Remote Sensing of Environment 259, 112411.

Hosseini, M., McNairn, H., Merzouki, A., Pacheco, A., 2015. Estimation of Leaf Area Index (LAI) in corn and soybeans using multi-polarization C- and L-band radar data. Remote Sensing of Environment 170, 77-89.

Huang, W., DeVries, B., Huang, C., Lang, M.W., Jones, J.W., Creed, I.F., Carroll, M.L., 2018. Automated Extraction of Surface Water Extent from Sentinel-1 Data. Remote Sensing 10(5).

Irwin, K., Braun, A., Fotopoulos, G., Roth, A., Wessel, B., 2018. Assessing Single-Polarization and Dual-Polarization TerraSAR-X Data for Surface Water Monitoring. Remote Sensing 10(6).

Jeong, G., Oeverdieck, H., Park, S.J., Huwe, B., Ließ, M., 2017. Spatial soil nutrients prediction using three supervised learning methods for assessment of land potentials in complex terrain. Catena 154, 73-84.

Kuhn, M., 2008. Building Predictive Models in R Using the caret Package. Journal of Statistical Software 28(5), 1-26.

Kumar, S., Babu, A., Agrawal, S., Asopa, U., Shukla, S., Maiti, A., 2022. Polarimetric calibration of spaceborne and airborne multifrequency SAR data for scattering-based characterization of manmade and natural features. Advances in Space Research 69(4), 1684-1714.

Lamichhane, S., Kumar, L., Wilson, B., 2019. Digital soil mapping algorithms and covariates for soil organic carbon mapping and their implications: A review. Geoderma 352, 395-413.

Li, X., Ding, J., Liu, J., Ge, X., Zhang, J., 2021. Digital Mapping of Soil Organic Carbon Using Sentinel Series Data: A Case Study of the Ebinur Lake Watershed in Xinjiang. Remote Sensing 13(4).

Liang, Z., Chen, S., Yang, Y., Zhou, Y., Shi, Z., 2019. High-resolution three-dimensional mapping of soil organic carbon in China: Effects of SoilGrids products on national modeling. Science of The Total Environment 685, 480-489.

Liu, D., Qi, Z., Zhang, H., Li, X., Yeh, A.G.-o., Wang, J., 2021. Investigation of the capability of multitemporal RADARSAT-2 fully polarimetric SAR images for land cover classification: a case of Panyu, Guangdong province. European Journal of Remote Sensing 54(1), 338-350.

Llamas, R.M., Guevara, M., Rorabaugh, D., Taufer, M., Vargas, R., 2020. Spatial Gap-Filling of ESA CCI Satellite-Derived Soil Moisture Based on Geostatistical Techniques and Multiple Regression, Remote Sensing.

Loiseau, T., Chen, S., Mulder, V.L., Román Dobarco, M., Richer-de-Forges, A.C., Lehmann, S., Bourennane, H., Saby, N.P.A., Martin, M.P., Vaudour, E., Gomez, C., Lagacherie, P., Arrouays, D., 2019. Satellite data integration for soil clay content modelling at a national scale. International Journal of Applied Earth Observation and Geoinformation 82, 101905.

Luo, C., Wang, Y., Zhang, X., Zhang, W., Liu, H., 2022a. Spatial prediction of soil organic matter content using multiyear synthetic images and partitioning algorithms. Catena 211, 106023.

Luo, C., Zhang, X., Meng, X., Zhu, H., Ni, C., Chen, M., Liu, H., 2022b. Regional mapping of soil organic matter content using multitemporal synthetic Landsat 8 images in Google Earth Engine. Catena 209, 105842.

Luo, C., Zhang, X., Wang, Y., Men, Z., Liu, H., 2022c. Regional soil organic matter mapping models based on the optimal time window, feature selection algorithm and Google Earth Engine. Soil and Tillage Research 219, 105325.

Ma, J., Kang, F., Cheng, X., Han, H., 2018. Response of soil organic carbon and nitrogen to nitrogen deposition in a Larix principis-rupprechtii plantation. Sci Rep 8(1), 8638.

Ma, Y., Minasny, B., Wu, C., 2017. Mapping key soil properties to support agricultural production in Eastern China. Geoderma Regional 10, 144-153.

Mahdavi, S., Amani, M., Maghsoudi, Y., 2019. The effects of orbit type on synthetic aperture RADAR (SAR) backscatter. Remote Sensing Letters 10(2), 120-128.

Mahdianpari, M., Salehi, B., Mohammadimanesh, F., Motagh, M., 2017. Random forest wetland classification using ALOS-2 L-band, RADARSAT-2 C-band, and TerraSAR-X imagery. ISPRS Journal of Photogrammetry and Remote Sensing 130, 13-31.

Maynard, J.J., Levi, M.R., 2017. Hyper-temporal remote sensing for digital soil mapping: Characterizing soil-vegetation response to climatic variability. Geoderma 285, 94-109.

McBratney, A.B., Mendonça Santos, M.L., Minasny, B., 2003. On digital soil mapping. Geoderma 117(1), 3-52.

Mengen, D., Montzka, C., Jagdhuber, T., Fluhrer, A., Brogi, C., Baum, S., Schüttemeyer, D., Bayat, B., Bogena, H., Coccia, A., Masalias, G., Trinkel, V., Jakobi, J., Jonard, F., Ma, Y., Mattia, F., Palmisano, D., Rascher, U., Satalino, G., Schumacher, M., Koyama, C., Schmidt, M., Vereecken, H., 2021. The SARSense Campaign: Air- and Space-Borne C- and L-Band SAR for the Analysis of Soil and Plant Parameters in Agriculture, Remote Sensing.

Minasny, B., McBratney, A.B., 2016. Digital soil mapping: A brief history and some lessons. Geoderma 264, 301-311.

Müller, M.M., Vacik, H., Diendorfer, G., Arpaci, A., Formayer, H., Gossow, H., 2013. Analysis of lightning-induced forest fires in Austria. Theoretical and Applied Climatology 111(1), 183-193.

Murphy, S.W., de Souza Filho, C.R., Wright, R., Sabatino, G., Correa Pabon, R., 2016. HOTMAP: Global hot target detection at moderate spatial resolution. Remote Sensing of Environment 177, 78-88.

Musche, M., Adamescu, M., Angelstam, P., Bacher, S., Bäck, J., Buss, H.L., Duffy, C., Flaim, G., Gaillardet, J., Giannakis, G.V., Haase, P., Halada, L., Kissling, W.D., Lundin, L., Matteucci, G., Meesenburg, H., Monteith, D., Nikolaidis, N.P., Pipan, T., Pyšek, P., Rowe, E.C., Roy, D.B., Sier, A., Tappeiner, U., Vilà, M., White, T., Zobel, M., Klotz, S., 2019. Research questions to facilitate the future development of European long-term ecosystem research infrastructures: A horizon scanning exercise. J Environ Manage 250, 109479.

Naimi, S., Ayoubi, S., Demattê, J.A.M., Zeraatpisheh, M., Amorim, M.T.A., Mello, F.A.d.O., 2022a. Spatial prediction of soil surface properties in an arid region using synthetic soil image and machine learning. Geocarto International 37(25), 8230-8253.

Naimi, S., Ayoubi, S., Di Raimo, L.A.D.L., Dematte, J.A.M., 2022b. Quantification of some intrinsic soil properties using proximal sensing in arid lands: Application of Vis-NIR, MIR, and pXRF spectroscopy. Geoderma Regional 28, e00484.

Nguyen, T.T., Pham, T.D., Nguyen, C.T., Delfos, J., Archibald, R., Dang, K.B., Hoang, N.B., Guo, W., Ngo, H.H., 2022. A novel intelligence approach based active and ensemble learning for agricultural soil organic carbon prediction using multispectral and SAR data fusion. Science of The Total Environment 804, 150187.

Nussbaum, M., Spiess, K., Baltensweiler, A., Grob, U., Keller, A., Greiner, L., Schaepman, M.E., Papritz, A., 2018. Evaluation of digital soil mapping approaches with large sets of environmental covariates. SOIL 4(1), 1-22.

Odebiri, O., Mutanga, O., Odindi, J., 2022a. Deep learning-based national scale soil organic carbon mapping with Sentinel-3 data. Geoderma 411, 115695.

Odebiri, O., Mutanga, O., Odindi, J., Naicker, R., 2022b. Modelling soil organic carbon stock distribution across different land-uses in South Africa: A remote sensing and deep learning approach. ISPRS Journal of Photogrammetry and Remote Sensing 188, 351-362.

Odebiri, O., Odindi, J., Mutanga, O., 2021. Basic and deep learning models in remote sensing of soil organic carbon estimation: A brief review. International Journal of Applied Earth Observation and Geoinformation 102, 102389.

Odhiambo, B.O., Kenduiywo, B.K., Were, K., 2020. Spatial prediction and mapping of soil pH across a tropical afro-montane landscape. Applied Geography 114, 102129.

Oduor, C.O., Karanja, N.K., Onwonga, R.N., Mureithi, S.M., Pelster, D., Nyberg, G., 2018. Enhancing soil organic carbon, particulate organic carbon and microbial biomass in semi-arid rangeland using pasture enclosures. BMC Ecol 18(1), 45.

Orgiazzi, A., Ballabio, C., Panagos, P., Jones, A., Fernández-Ugalde, O., 2018. LUCAS Soil, the largest expandable soil dataset for Europe: a review. Eur J Soil Sci 69(1), 140-153.

Ottoy, S., De Vos, B., Sindayihebura, A., Hermy, M., Van Orshoven, J., 2017. Assessing soil organic carbon stocks under current and potential forest cover using digital soil mapping and spatial generalisation. Ecol Indicators 77, 139-150.

Peng, G., Bing, W., Guangpo, G., Guangcan, Z., 2014. Spatial Distribution of Soil Organic Carbon and Total Nitrogen Based on GIS and Geostatistics in a Small Watershed in a Hilly Area of Northern China. PLoS One 8(12), e83592.

Poggio, L., Gimona, A., 2017. Assimilation of optical and radar remote sensing data in 3D mapping of soil properties over large areas. Science of The Total Environment 579, 1094-1110.

Rapinel, S., Betbeder, J., Denize, J., Fabre, E., Pottier, É., Hubert-Moy, L., 2020. SAR analysis of wetland ecosystems: Effects of band frequency, polarization mode and acquisition dates. ISPRS Journal of Photogrammetry and Remote Sensing 170, 103-113.

Roca, M., Navarro, G., García-Sanabria, J., Caballero, I., 2022. Monitoring Sand Spit Variability Using Sentinel-2 and Google Earth Engine in a Mediterranean Estuary, Remote Sensing.

Schiefer, J., Lair, G.J., Blum, W.E.H., 2016. Potential and limits of land and soil for sustainable intensification of European agriculture. Agric, Ecosyst Environ 230, 283-293.

Shafizadeh-Moghadam, H., Minaei, F., Talebi-khiyavi, H., Xu, T., Homaee, M., 2022. Synergetic use of multi-temporal Sentinel-1, Sentinel-2, NDVI, and topographic factors for estimating soil organic carbon. Catena 212, 106077.

Shi, P., Six, J., Sila, A., Vanlauwe, B., Van Oost, K., 2022. Towards spatially continuous mapping of soil organic carbon in croplands using multitemporal Sentinel-2 remote sensing. ISPRS Journal of Photogrammetry and Remote Sensing 193, 187-199.

Singha, M., Dong, J., Sarmah, S., You, N., Zhou, Y., Zhang, G., Doughty, R., Xiao, X., 2020. Identifying floods and flood-affected paddy rice fields in Bangladesh based on Sentinel-1 imagery and Google Earth Engine. ISPRS Journal of Photogrammetry and Remote Sensing 166, 278-293.

Sleziak, P., Szolgay, J., Hlavčová, K., Parajka, J.J.S.J.o.C.E., 2016. The impact of the variability of precipitation and temperatures on the efficiency of a conceptual rainfall-runoff model. Slovak Journal of Civil Engineering 24(4), 1-7.

Surer, S., Parajka, J., Akyurek, Z., 2014. Validation of the operational MSG-SEVIRI snow cover product over Austria. Hydrol. Earth Syst. Sci. 18(2), 763-774.

Tamiminia, H., Salehi, B., Mahdianpari, M., Quackenbush, L., Adeli, S., Brisco, B., 2020. Google Earth Engine for geo-big data applications: A meta-analysis and systematic review. ISPRS Journal of Photogrammetry and Remote Sensing 164, 152-170.

Tian, F., Cai, Z., Jin, H., Hufkens, K., Scheifinger, H., Tagesson, T., Smets, B., Van Hoolst, R., Bonte, K., Ivits, E., Tong, X., Ardö, J., Eklundh, L., 2021. Calibrating vegetation phenology from Sentinel-2 using eddy covariance, PhenoCam, and PEP725 networks across Europe. Remote Sensing of Environment 260, 112456.

Tóth, G., Jones, A., Montanarella, L., 2013. The LUCAS topsoil database and derived information on the regional variability of cropland topsoil properties in the European Union. Environ Monit Assess 185(9), 7409-7425.

Tziolas, N., Tsakiridis, N., Ogen, Y., Kalopesa, E., Ben-Dor, E., Theocharis, J., Zalidis, G., 2020. An integrated methodology using open soil spectral libraries and Earth Observation data for soil organic carbon estimations in support of soil-related SDGs. Remote Sensing of Environment 244, 111793.

Vågen, T.-G., Winowiecki, L.A., Tondoh, J.E., Desta, L.T., Gumbricht, T., 2016. Mapping of soil properties and land degradation risk in Africa using MODIS reflectance. Geoderma 263, 216-225.

Vaudour, E., Gomez, C., Fouad, Y., Lagacherie, P., 2019. Sentinel-2 image capacities to predict common topsoil properties of temperate and Mediterranean agroecosystems. Remote Sensing of Environment 223, 21-33.

Wadoux, A.M.J.C., 2019. Using deep learning for multivariate mapping of soil with quantified uncertainty. Geoderma 351, 59-70.

Wadoux, A.M.J.C., Padarian, J., Minasny, B., 2019. Multi-source data integration for soil mapping using deep learning. SOIL 5(1), 107-119.

Wan, J.-Z., Yu, J.-H., Yin, G.-J., Song, Z.-M., Wei, D.-X., Wang, C.-J., 2019. Effects of soil properties on the spatial distribution of forest vegetation across China. Global Ecology and Conservation 18, e00635.

Wang, B., Waters, C., Orgill, S., Cowie, A., Clark, A., Li Liu, D., Simpson, M., McGowen, I., Sides, T., 2018. Estimating soil organic carbon stocks using different modelling techniques in the semi-arid rangelands of eastern Australia. Ecol Indicators 88, 425-438.

Wang, H., Zhang, X., Wu, W., Liu, H., 2021. Prediction of Soil Organic Carbon under Different Land Use Types Using Sentinel-1/-2 Data in a Small Watershed. Remote Sensing 13(7).

Wang, L., Diao, C., Xian, G., Yin, D., Lu, Y., Zou, S., Erickson, T.A., 2020a. A summary of the special issue on remote sensing of land change science with Google earth engine. Remote Sensing of Environment 248, 112002.

Wang, X., Zhang, Y., Atkinson, P.M., Yao, H., 2020b. Predicting soil organic carbon content in Spain by combining Landsat TM and ALOS PALSAR images. International Journal of Applied Earth Observation and Geoinformation 92, 102182.

Yagüe-Martínez, N., Prats-Iraola, P., González, F.R., Brcic, R., Shau, R., Geudtner, D., Eineder, M., Bamler, R., 2016. Interferometric Processing of Sentinel-1 TOPS Data. IEEE Transactions on Geoscience and Remote Sensing 54(4), 2220-2234.

Yang, L., Cai, Y., Zhang, L., Guo, M., Li, A., Zhou, C., 2021. A deep learning method to predict soil organic carbon content at a regional scale using satellite-based phenology variables. International Journal of Applied Earth Observation and Geoinformation 102, 102428.

Yang, R.-M., Guo, W.-W., Zheng, J.-B., 2019. Soil prediction for coastal wetlands following Spartina alterniflora invasion using Sentinel-1 imagery and structural equation modeling. Catena 173, 465-470.

Yigini, Y., Panagos, P., 2016. Assessment of soil organic carbon stocks under future climate and land cover changes in Europe. Science of The Total Environment 557-558, 838-850.

Zeraatpisheh, M., Ayoubi, S., Jafari, A., Tajik, S., Finke, P., 2019. Digital mapping of soil properties using multiple machine learning in a semi-arid region, central Iran. Geoderma 338, 445-452.

Zeraatpisheh, M., Garosi, Y., Reza Owliaie, H., Ayoubi, S., Taghizadeh-Mehrjardi, R., Scholten, T., Xu, M., 2022. Improving the spatial prediction of soil organic carbon using environmental covariates selection: A comparison of a group of environmental covariates. Catena 208, 105723.

Zhang, G.-l., Liu, F., Song, X.-d., 2017. Recent progress and future prospect of digital soil mapping: A review. Journal of Integrative Agriculture 16(12), 2871-2885.

Zhang, W., Brandt, M., Wang, Q., Prishchepov, A.V., Tucker, C.J., Li, Y., Lyu, H., Fensholt, R., 2019. From woody cover to woody canopies: How Sentinel-1 and Sentinel-2 data advance the mapping of woody plants in savannas. Remote Sensing of Environment 234, 111465.

Zhang, X., Zhang, F., Wang, D., Fan, J., Hu, Y., Kang, H., Chang, M., Pang, Y., Yang, Y., Feng, Y., 2018. Effects of vegetation, terrain and soil layer depth on eight soil chemical properties and soil fertility based on hybrid methods at urban forest scale in a typical loess hilly region of China. PLoS One 13(10), e0205661.

Zhang, Y., Ji, W., Saurette, D.D., Easher, T.H., Li, H., Shi, Z., Adamchuk, V.I., Biswas, A., 2020. Three-dimensional digital soil mapping of multiple soil properties at a field-scale using regression kriging. Geoderma 366, 114253.

Zhou, T., Geng, Y., Chen, J., Pan, J., Haase, D., Lausch, A., 2020. High-resolution digital mapping of soil organic carbon and soil total nitrogen using DEM derivatives, Sentinel-1 and Sentinel-2 data based on machine learning algorithms. Science of The Total Environment 729, 138244.

Zhou, T., Geng, Y., Ji, C., Xu, X., Wang, H., Pan, J., Bumberger, J., Haase, D., Lausch, A., 2021. Prediction of soil organic carbon and the C:N ratio on a national scale using machine learning and satellite data: A comparison between Sentinel-2, Sentinel-3 and Landsat-8 images. Science of The Total Environment 755, 142661.

Zhou, Y., Zhao, X., Guo, X., Li, Y., 2022. Mapping of soil organic carbon using machine learning models: Combination of optical and radar remote sensing data. Soil Science Society of America Journal 86(2), 293-310.